Catalysis Today 137 (2008) 90–102

Contents lists available at ScienceDirect

Catalysis Today

journal homepage: www.elsevier.com/locate/cattod

Microkinetics of methane oxidative coupling

Jianjun Sun, Joris W. Thybaut *, Guy B. Marin

Laboratory or Chemical Technology, Ghent University, Krijgslaan 281-S5, B-9000 Ghent, Belgium

ARTICLE INFO

Article history:
Available online 24 April 2008

Keywords:
Methane
Oxidative coupling
Natural gas
Catalyst descriptor
High throughput
Microkinetics
Modeling

ABSTRACT

A detailed microkinetic model for methane oxidative coupling has been developed including so-called catalyst descriptors. The reaction network contains 39 elementary steps describing the gas-phase reactions and 14 catalytic reactions. The model has been implemented in a one-dimensional heterogeneous reactor model, which accounts for the interactions between the species in the gas phase and inside the catalyst pores. Based on the proposed reaction mechanism, catalyst descriptors of methane oxidative coupling have been identified and incorporated into the microkinetic model through the use of Polanyi relationships for the reaction families of catalytic reactions encountered in the reaction network. The application of catalyst descriptors for two catalysts, Li/MgO and Sn/Li/MgO, has been used as an example to illustrate the model performance. The simulations are consistent with the experimental results over a broad range of operating conditions. This is a first validation of the description of experimental data on a family of catalysts with a single kinetic model including catalyst descriptors that can capture the trends in productivity and selectivity on different catalysts. This microkinetic model with catalyst descriptors can be used as an effective tool to extract knowledge from high-throughput experiments of methane oxidative coupling.

1. Introduction

Oxidative coupling of methane (OCM) has been investigated extensively as a possible direct process to convert natural gas to valuable products [1,2]. It is generally accepted that OCM is a catalytic and gas-phase reaction process [3–7]. A general scheme of the reactions involving reactants and products is shown in Fig. 1. Gas-phase reactions involve radicals and are responsible for the most important step of OCM, i.e., the coupling of two methyl radicals leading to ethane. The reaction mechanism on the catalyst surface of OCM is very complex. Oxygen is required to activate the catalyst and interacts strongly with the surface by dissociative reversible adsorption [8–10]. An OCM catalyst acts not only as the radical initiator but also as the radical quencher. The importance of the different pathways of the non-selective oxidation on the surface varies with the operating conditions [11]. The adsorption of CO_2 is reported to inhibit the OCM reactions [12,13].

Microkinetic analyses have been applied to study the reaction mechanism of and the transport limitations in OCM by different researchers. In the microkinetic models, initial estimates for kinetic parameters were obtained using physico-chemical relations and thermodynamic constraints [14,15]. A Polanyi relationship for the activation of methane on different catalysts was derived from a kinetic model consisting of elementary steps with the kinetic parameters adjusted to experimental data [16,17]. Relations between the surface composition and the rate coefficients were determined based on an elementary kinetic model for methane oxidative coupling at low conversions [18,19]. A theoretical estimation of the upper bound of C_2 yields has also been carried out with a detailed microkinetic model [20]. In the microkinetic models of OCM, combining catalytic reactions with gas-phase reactions is necessary to describe the full features of the reactions and transport of components in the reactor. By implementing the microkinetic model in a one-dimensional heterogeneous reactor model, the interaction between gas phase and catalytic reactions of OCM could explicitly be taken into account in the model developed by Couwenberg et al. [21,22], which provides a solid base for the present work.

High-throughput experimentation provides the capability to accelerate the discovery and development of new catalysts and it has received a growing interest from different research labs and industrial companies [23–26]. It has been widely applied in the area of petroleum chemistry and medicine research and a variety of cases have been summarized in several reviews [23–25]. High-throughput experimentation in catalysis includes the synthesis of catalyst libraries, experimental characterization of the catalytic activity and the analysis of the data obtained [24,27]. Specifically designed equipments have been constructed for automatic and

* Corresponding author. Tel.: +32 9 264 45 19; fax: +32 9 264 49 99.
E-mail address: Joris.Thybaut@UGent.be (J.W. Thybaut).

0920-5861/$ – see front matter © 2008 Elsevier B.V. All rights reserved.
doi:10.1016/j.cattod.2008.02.026

Nomenclature

A	pre-exponential factor (Arrhenius), reaction dependent
B	parameter vector
$C_{1/2}$	component contain one carbon atom or two carbon atoms
D	catalyst descriptor, unit is property dependent
E_0	intrinsic activation barrier (kJ mol^{-1})
E_a	activation energy (J mol^{-1})
F	ratio of mean regression sum of squares to the residual sum of squares
$F_{t,0}$	molar flow rate (mol s^{-1})
h	Plank constant (J s^{-1})
ΔH_r	reaction enthalpy (kJ mol^{-1})
ΔH_f°	standard formation enthalpy (kJ mol^{-1})
k	rate coefficient, reaction dependent
k_b	Boltzmann constant (J K^{-1})
K	equilibrium coefficient, reaction dependent
M_i	molar mass of component i (kg mol^{-1})
P	pressure (Pa)
Q_{H-CH_3}	C–H bond energies of methane (kJ mol^{-1})
$Q_{H-C_2H_5}$	C–H bond energies of ethane (kJ mol^{-1})
$Q_{H-C_2H_3}$	C–H bond energies of ethylene (kJ mol^{-1})
r_i	rate of reaction i (mol m$^{-3}{}_g$ s^{-1})
R	the universal gas constant (J mol^{-1} K^{-1})
S	sensitivity coefficient
S_0	initial sticking probability
T	temperature (K)
W	catalyst mass (kg)
X_i	conversion of component i
y	observed molar fraction at the reactor outlet
$\hat{y}$	calculated molar fraction at the reactor outlet

Greek letters

α	transfer coefficient of Polanyi parameter
σ	active site density
φ^{-1}	an element of the inverse of the error variance–covariance matrix

Subscript

c	catalyst pellet

Superscripts

b	backward reaction step
f	forward reaction step

systematic synthesis of catalyst libraries. Different strategies have been proposed to guide the design of high-throughput experiments [26,27]. Set-ups that contain parallel and micro reactors enable testing catalysts in a high-throughput way. A variety of analytical tools such as infrared thermography, improved mass spectrometry and gas chromatography, etc., have been applied in high-throughput experiments to collect the analytical data simultaneously or in a short period. In the data analysis of high-throughput experiments, knowledge extraction is an important task [28]. Different mathematical tools such as clustering techniques, genetic algorithms and artificial neural networks etc. are available to perform the knowledge extraction [26,27,29]. With these tools, quantitative structure/property relationship modeling that provide predicting capabilities has been successfully applied to several cases [26,29]. But this kind of approach, however, does not explicitly accounts for or utilizes the underlying chemistry of the process in terms of elementary steps. The use of microkinetic models in high-throughput experimentation and modeling allows better exploitation of the fundamental knowledge of the chemistry of the process in catalyst design and optimization.

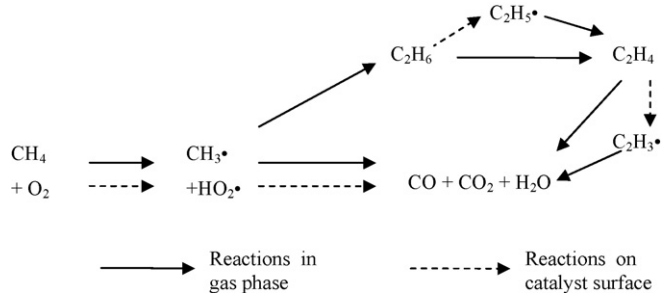

Fig. 1. A general scheme of the reaction network in oxidative coupling of methane.

High-throughput technology in chemical kinetic data acquisition also denoted as combinatorial chemistry has proved to be an effective tool to accelerate catalysis research. As high-throughput technology is able to provide the quantitative information of the catalyst performance [28,30], one approach of combining microkinetic analyses with combinatorial chemistry in the iterative process of catalyst evaluation and evolution has been proposed for assisted catalyst design [31]. The microkinetic analysis is based on the analysis of catalytic cycles on the catalyst surface and describes the reaction in terms of elementary reactions involving adsorbed reactants, products, and reaction intermediates associated with active sites [32,33]. Not assuming any rate-determining step results in highly flexible models to describe the surface chemistry with varying operating conditions and different catalysts. Moreover, the kinetic parameters of the microkinetic model can be related with the physical and chemical catalyst properties, also denoted as catalyst descriptors. The latter represent the essential differences between the various candidate catalysts.

A useful tool for the incorporation of catalyst descriptors in microkinetic models is the Polanyi relationship, which relates the reaction enthalpy with the activation energy of the reaction

$$E_a^f = E_0 + \alpha \Delta H_r \quad (1)$$

where α is the so-called transfer coefficient of Polanyi relationship, ΔH_r is the reaction enthalpy of the elementary reaction and E_0 is the intrinsic activation barrier. It has been shown that this relation exists for different elementary heterogeneous reactions, such as the adsorbate dehydrogenation and dissociation of CO, CO_2 and NH_3, etc. on transition metals [34,35]. It has also been applied to the different microkinetic models [26].

The implementation of thermodynamic relationships in a microkinetic model allows relating model parameters to catalyst descriptors. For surface reaction mechanisms, an important feature of thermodynamic relationships is that the heats of surface reactions can be derived from the heats of formation of surface species and heats of analogous gas-phase reactions [36], which guarantee the thermodynamic consistency. Applying thermodynamic consistency through thermodynamic cycles allows to express reaction enthalpies for various elementary steps as a function of a limited number of unknown parameters which will then be obtained, e.g., by regression. Mhadeshwar

et al. [36] have demonstrated the use of various methods to apply thermodynamic relationships in microkinetic models with several examples: hydrogenation of ethylene, H_2 oxidation on Pt and the ammonia synthesis. Another example of applying thermodynamic cycles is a theoretical analysis of OCM catalyst performance [20].

The present day reported microkinetic models in the literature are focused on either the description of conversion and selectivity of OCM catalysts or on the explanation of specific catalytic reaction pathways in OCM, but not on the treatment of high-throughput experimental data. For a microkinetic model of OCM to provide useful catalyst information which can be used as a guide line for the design of new catalyst generations, the reaction mechanism of OCM on catalyst surface should be constructed in full detail, instead of only emphasizing the important products of OCM. For instance, the reactions on OCM catalysts also involve CO oxidation and H_2 production. Actually, a well-designed OCM catalyst might, under appropriate operating conditions, be combined with other reactions to provide other pathways for the utilisation of natural gas [37].

The aim of the present work was to develop a kinetic model that is able to describe the large amount of data of different catalysts produced by high-throughput technology. For this purpose, a microkinetic model was developed for methane oxidative coupling and catalyst descriptors were incorporated. This microkinetic model incorporated into a one-dimensional heterogeneous reactor model was firstly validated for a tin promoted lithium on magnesium oxide catalyst over a wide range of process conditions, and subsequently for the original Li MgO catalyst. The kinetic model comprises the elementary catalytic reactions coupled to a gas-phase reaction network reported by Chen et al. [38,39]. The catalytic elementary steps are based on steady state kinetic experiments, temporal analysis of products (TAP) experiments [21,40–42] and steady-state transient isotopic kinetic (SSITKA) experiments [43] with the catalysts that have the same composition.

2. Procedures

2.1. Experimental details

The experimental data used in this study were obtained from the previous work [21,22]. The experiments were performed in a fixed bed reactor. The operating conditions and catalyst properties are given in Table 1.

2.2. Reactor model

The kinetic model has been implemented in a one-dimensional heterogeneous reactor model [22]. The latter model consists of a set of partial differential equations to calculate the concentration profiles in both the gas phase and the pores of the solid phase. Also the interactions between the catalytic elementary steps and the gas-phase reactions are explicitly accounted for. Orthogonal collocation is used to transform the equations to a set of ordinary differential equations coupled with algebraic equations. The resulting simulation model is applicable over a broad range of operating conditions.

Table 1
Experimental operating conditions and catalyst properties

Pressure (kPa)	108.0–130.0
Temperature (K)	947.0–1013.0
CH_4/O_2 (mol mol^{-1})	2.0–12.0
$W/F_{t,0}$ (kg mol^{-1} s)	2.0–12.0
Diameter of catalyst pellet (m)	2.5×10^{-4}
Catalyst	
Sn/Li/MgO	
BET surface area (m^2 kg^{-1})	2800.0
Porosity	0.27
Density (kg m^{-3})	2300.0
Li/MgO	
BET surface area (m^2 kg^{-1})	1000.0
Porosity	0.29
Density (kg m^{-3})	2350.0

2.3. Parameter estimation and sensitivity analysis

The Rosenbrock method [44] was used for the initial minimization of the objective function in the model regression and the obtained result was refined by applying ODRPACK-package version 2.01 [45], in which the Marquardt method has been implemented. The objective function used in the model is the weighed sum of the squared residuals, $S(b)$ between the observed, y, and calculated, $\hat{y}$, mole fractions at the reactor outlet

$$S(b) = \sum_{j=1}^{\text{nresp}} \sum_{k=1}^{\text{nresp}} \varphi_{j,k}^{-1} \sum_{i=1}^{\text{nobs}} (y_{i,j} - \hat{y}_{i,j})(y_{i,k} - \hat{y}_{i,k}) \xrightarrow{b} \min \quad (2)$$

where b is the parameter vector containing catalyst descriptors; $\varphi_{j,k}^{-1}$ is an element of the inverse of the error variance–covariance matrix, which is calculated from replicate experiments or estimated from the observed and calculated molar fractions at the reactor outlet. The objective function was minimized by adjusting the model parameter vector b.

A sensitivity analysis can help identifying the important parameters in the microkinetic model. The first-order sensitivity coefficient for reactant conversion or product selectivity on the parameters of the microkinetic model is defined according to

$$S_{i,j} = \frac{D_i}{\mathrm{d}D_i} \frac{\mathrm{d}y_j}{y_j} \approx \frac{D_i}{\Delta D_i} \frac{\Delta y_j}{y_j} \quad (3)$$

where D_i represents the parameter i in the microkinetic model and refers to catalyst descriptor introduced in Section 4; y_j is the molar fraction of species j at the outlet of the reaction; ΔD_i and Δy_i are approximated as a small fraction of D_i or y_i. In this case, the fraction is set as 0.001.

3. Microkinetic model development

The microkinetic model accounts for the gas-phase kinetics as well as for the catalytic reactions in methane oxidative coupling. The gas-phase kinetics contain 39 elementary reactions among 13 molecules and 10 radicals. A catalytic reaction network has been developed in terms of 14 elementary steps and 9 surface species. The values of kinetic parameters were obtained by collision theory, transition state theory, thermochemical relations and, finally, regression.

3.1. Gas-phase mechanism

A detailed kinetic model for gas-phase reactions of methane oxidative coupling was adopted [39,46]. The reaction network for methane oxidative coupling in the absence of catalyst is shown in Table 2. The molecules are: dihydrogen, water, hydrogen peroxide, dioxygen, methane, methanal, carbon monoxide, carbon dioxide, ethyne, ethene, ethane, propene, and propane. The radicals are: hydrogen and oxygen atoms, hydroxyl, hydrogen peroxy, formyl, methoxy radicals and methyl, vinyl, ethyl, and propyl radicals. The parameters of the model have been fitted with the experimental data. The Arrhenius equation (Eq. (4)) is used to calculate the reaction constant and the pre-exponential factor and the activation energy for the forward step of each reaction are also given in

Table 2
Elementary steps considered in the gas phase in the oxidative coupling of methane and corresponding parameter values [39,46]

Reaction	A (s^{-1} or $m^3\ mol^{-1}\ s^{-1}$ or $m^6\ mol^{-2}\ s^{-1}$)	E_a (kJ mol^{-1})
$CH_4 + O_2 \rightarrow CH_3^\bullet + HO_2^\bullet$ (1)	0.983×10^7	193.86
$CH_4 + H^\bullet \rightarrow CH_3^\bullet + H_2$ (2)	0.234×10^9	51.17
$CH_4 + O^\bullet \rightarrow CH_3^\bullet + OH^\bullet$ (3)	0.127×10^{10}	33.83
$CH_4 + OH^\bullet \rightarrow CH_3^\bullet + H_2O$ (4)	0.743×10^9	41.43
$CH_4 + HO_2^\bullet \rightarrow CH_3^\bullet + H_2O_2$ (5)	0.401×10^8	99.61
$CH_3^\bullet + O_2 \rightarrow CH_3O^\bullet + O^\bullet$ (6)	0.308×10^9	141.00
$CH_3^\bullet + O_2 \rightarrow CH_2O + OH^\bullet$ (7)	0.459×10^8	103.66
$CH_3^\bullet + HO_2^\bullet \rightarrow CH_3O^\bullet + OH^\bullet$ (8)	0.885×10^8	0.00
$CH_3^\bullet + CH_3^\bullet + M \rightarrow C_2H_6 + M$ (9)	0.650×10^8	0.00
$CH_3O^\bullet + M \rightarrow CH_2O + H^\bullet + M$ (10)	0.258×10^{15}	115.00
$CH_2O + OH^\bullet \rightarrow CHO^\bullet + H_2O$ (11)	0.580×10^9	5.00
$CH_2O + HO_2^\bullet \rightarrow CHO^\bullet + H_2O_2$ (12)	0.417×10^7	40.12
$CH_2O + CH_3^\bullet \rightarrow CHO^\bullet + CH_4$ (13)	0.700×10^8	25.03
$CHO^\bullet + M \rightarrow CO + H^\bullet + M$ (14)	0.280×10^{10}	64.36
$CHO^\bullet + O_2 \rightarrow CO + HO_2^\bullet$ (15)	0.171×10^6	0.00
$CO + HO_2^\bullet \rightarrow CO_2 + OH^\bullet$ (16)	0.308×10^9	107.34
$C_2H_6 + H^\bullet \rightarrow C_2H_5^\bullet + H_2$ (17)	0.910×10^9	51.70
$C_2H_6 + OH^\bullet \rightarrow C_2H_5^\bullet + H_2O$ (18)	0.545×10^9	17.16
$C_2H_6 + CH_3^\bullet \rightarrow C_2H_5^\bullet + CH_4$ (19)	0.239×10^8	64.73
$C_2H_5^\bullet + HO_2^\bullet \rightarrow CH_3^\bullet + CH_2O + OH^\bullet$ (20)	0.948×10^7	0.00
$C_2H_5^\bullet + M \rightarrow C_2H_4 + H^\bullet + M$ (21)	0.596×10^{14}	167.66

Table 2 (*Continued*)

Reaction	A (s^{-1} or $m^3\ mol^{-1}\ s^{-1}$ or $m^6\ mol^{-2}\ s^{-1}$)	E_a (kJ mol^{-1})
$C_2H_5^\bullet + O_2 \rightarrow C_2H_4 + HO_2^\bullet$ (22)	0.635×10^7	53.20
$C_2H_4 + O_2 \rightarrow C_2H_3^\bullet + HO_2^\bullet$ (23)	0.281×10^7	144.55
$C_2H_4 + H^\bullet \rightarrow C_2H_3^\bullet + H_2$ (24)	0.150×10^9	42.70
$C_2H_4 + OH^\bullet \rightarrow C_2H_3^\bullet + H_2O$ (25)	0.612×10^8	24.70
$C_2H_4 + CH_3^\bullet \rightarrow C_2H_3^\bullet + CH_4$ (26)	0.199×10^6	51.46
$C_2H_4 + OH^\bullet \rightarrow CH_3^\bullet + CH_2O$ (27)	0.272×10^7	0.00
$C_2H_3^\bullet + M \rightarrow C_2H_2 + H^\bullet + M$ (28)	0.121×10^{16}	176.44
$C_2H_3^\bullet + O_2 \rightarrow C_2H_2 + HO_2^\bullet$ (29)	0.500×10^7	0.00
$C_2H_3^\bullet + O_2 \rightarrow CH_2O + CHO^\bullet$ (30)	0.550×10^7	0.00
$C_2H_5^\bullet + CH_3^\bullet \rightarrow C_3H_8$ (31)	0.800×10^7	0.00
$C_3H_8 + H^\bullet \rightarrow C_3H_7^\bullet + H_2$ (32)	0.900×10^9	32.00
$C_2H_4 + CH_3^\bullet \rightarrow C_3H_7^\bullet$ (33)	0.300×10^6	29.00
$C_3H_7^\bullet \rightarrow C_3H_6 + H^\bullet$ (34)	0.150×10^{16}	156.00
$O_2 + H^\bullet \rightarrow OH^\bullet + O^\bullet$ (35)	0.220×10^9	70.30
$O_2 + H^\bullet + M \rightarrow HO_2^\bullet + M$ (36)	0.139×10^6	0.00
$HO_2^\bullet + HO_2^\bullet \rightarrow O_2 + OH^\bullet + OH^\bullet$ (37)	0.200×10^{07}	0.00
$H_2O_2 + M \rightarrow OH^\bullet + OH^\bullet + M$ (38)	0.127×10^{12}	199.36
$C_2H_6 \rightarrow C_2H_5^\bullet + H^\bullet$ (39)	0.400×10^{17}	378.51

Conditions used in the experiments used for determining the reported parameter values: are reported in Table 1; X_{CH4}, 0.07–0.26; X_{O_2}, 0.20–0.98.

Table 2. The forward rate coefficient of reaction i, k_i^f, can be calculated from the Arrhenius equation:

$$k_i^f = A_i^f \exp\left(-\frac{E_{a,i}^f}{RT}\right) \quad (4)$$

where A_i^f is the pre-exponential factor and $E_{a,i}^f$ is the activation energy for the forward direction of the ith reaction. The rate coefficient for the backward direction, k_i^b, is calculated by means of the equilibrium coefficient K_i and the forward rate coefficient k_i^f:

$$k_i^b = A_i^b \exp\left(-\frac{E_{a,i}^b}{RT}\right) = \frac{A_i^f \exp(-(E_{a,i}^f/RT))}{K_i} \quad (5)$$

where k_i^b and $E_{a,i}^b$ are the pre-exponential factor and the activation energy of the backward step, respectively; K_i is calculated at a given temperature by using the Chemkin

Table 3
Catalytic elementary reactions considered in the oxidative coupling of methane and corresponding parameter values for Sn/Li/MgO (Parameters are calculated from Eqs. (7) to (13) and the values of catalyst descriptors of Sn/Li/MgO listed in Table 6)

Elementary reaction	A^f or S_0	E_a^f	A^b or S_0	E_a^b
$O_2 + 2* \rightleftharpoons 2O*$ (40)	0.4 (D_8)	0.0	2.39×10^{15}	110.7 (D_2)
$CH_4 + O* \rightleftharpoons CH_3^\bullet + OH*$ (41)	1.85×10^{07}	146.4	1.91×10^{07}	85.0
$C_2H_4 + O* \rightleftharpoons C_2H_3^\bullet + OH*$ (42)	1.40×10^{07}	131.4	1.42×10^{07}	90.1
$C_2H_6 + O* \rightleftharpoons C_2H_5^\bullet + OH*$ (43)	1.35×10^{07}	166.2	1.37×10^{07}	78.5
$2OH* \rightleftharpoons H_2O* + O*$ (44)	2.25×10^{15}	190.3	2.17×10^{15}	98.2
$H_2O* \rightleftharpoons H_2O + OH + *$ (45)	2.10×10^{13}	54.2 (D_7)	0.52 (D_{12})	0.0
$CH_3^\bullet + O* \rightleftharpoons CH_3O*$ (46)	3.3×10^{-5} (D_9)	0.0	2.24×10^{13}	244.6
$CH_3O* + O* \rightleftharpoons CH_2O* + OH*$ (47)	1.72×10^{15}	0.0	1.69×10^{15}	155.9
$CH_2O* + O* \rightleftharpoons HCO* + OH*$ (48)	1.69×10^{15}	35.1	1.75×10^{15}	112.6
$CHO* + O* \rightleftharpoons CO* + OH*$ (49)	1.75×10^{15}	14.7	1.81×10^{15}	133.9
$CO* + O* \rightleftharpoons CO_2* + *$ (50)	1.81×10^{15}	0.0	1.39×10^{15}	205.3
$CO + * \rightleftharpoons CO*$ (51)	2.7×10^{-4} (D_{10})	0.0	1.81×10^{13}	101.4 (D_5)
$CO_2 + * \rightleftharpoons CO_2*$ (52)	0.01 (D_{11})	0.0	1.07×10^{13}	160.9 (D_6)
$4HO_2^\bullet \xrightarrow{surf} 3O_2 + 2H_2O$ (53)	1.0×10^{-2}			

(*) Represents the active site on the catalyst surface. Units: A, $m^3\ mol^{-1}\ s^{-1}$((41)$^{f+b}$, (42)$^{f+b}$, (43)$^{f+b}$, (45)^b, (46)^f, (51)^f, (52)^f); $m^2\ mol^{-1}\ s^{-1}$((44)$^{f+b}$, (47)$^{f+b}$, (48) $^{f+b}$, (49)$^{f+b}$, (50)$^{f+b}$); $m^5\ mol^{-2}\ s^{-1}$(40)^b, s^{-1} ((45)^f, (46)^b, (51)^b, (52)^b); $m^3\ m_c^{-2}\ s^{-1}$ (53). E_a, kJ mol^{-1}. E_a of reaction (41), (42), (43) are calculated from the catalyst descriptor, D_1 and reaction family 1; 44, D_1, D_2, D_7 and reaction family 3; 47, 48, 49, D_1, D_2, D_3, D_4, D_5 and reaction family 2; 50, D_2, D_5, D_6 and reaction family 4.

thermodynamic data base of the Sandia National Laboratory [47].

3.2. Catalytic reaction network

The reaction mechanism of methane oxidative coupling on different catalysts has been studied by means of various techniques [5,6,11,42,43,48–54] and several general catalyst functions have been identified:

- Oxygen activation;
- Generation of radicals;
- Non-selective oxidation on catalyst surface;
- Radical quenching;
- Inhibition by CO_2.

The reaction network representing these functions in methane oxidative coupling is listed in the first column of Table 3 and is used in the simulation of OCM. The other columns of Table 3 contain the values of pre-exponential factors and activation energies determined from catalyst descriptors of OCM in Section 4. The catalyst descriptors are defined in Section 4.1 and relationships between catalyst descriptors and model parameters are explained in Section 4.2. Finally, the catalyst descriptor values are determined by regression. The rate coefficients are calculated from Eq. (4) and include also the effect of the density of active sites. The following equation is used for computing the rate coefficient k of adsorption steps with assuming that these steps are non-activated ones [47]:

$$k_i = \frac{S_{0,i}}{\sigma^n}\sqrt{\frac{RT}{2\pi M}} \quad (6)$$

where k_i is the rate coefficient of catalytic reaction i, mol $m^{-2}\ s^{-1}$; R is the universal gas constant; T is temperature, K; M is molar mass, kg mol^{-1}; σ is the density of active sites, mol m^{-2}; n is the reaction

order; S_0, the initial sticking probability, that is the probability molecules are trapped on a clean surface of the catalyst and chemisorbed.

It has been well established that the oxygen surface species are responsible for the activation of methane and that oxygen has a strong interaction with the OCM catalyst by a dissociative adsorption process [10,43,51,54]. A static equilibrium among the gaseous oxygen, surface oxygen species and lattice oxygen species has been observed. The exact nature and function of surface oxygen species, however, is still a matter of debate. Different oxygen surface species, such as O^- [6], the superoxide anion O^{2-}, the peroxide anion O_2^{2-}, and the ozonide anion O^{3-} [49,55] have been identified on the catalyst surface and mentioned as the active species for methane hydrogen abstraction. A two-step mechanism has been reported for the adsorption of oxygen on the catalyst surface, in which the adsorption of dioxygen on a vacant site is followed by its dissociation to form two atomic oxygen species [15,56,57]. The complex ionic structures occurring in these adsorption steps make the determination of the dissociation energy difficult. Moreover, it was found that a one-step dissociative adsorption of oxygen sufficiently described the experimental data with varying the inlet methane-to-oxygen ratio [21,43]. Therefore, one-step oxygen dissociative adsorption with reaction (40) was assumed and the adsorbed oxygen, O*, was considered as the active species in hydrogen abstraction of methane.

The activation of methane occurs through the breaking of a C–H bond assisted by an adsorbed oxygen species, O*, and leads to a methyl radical [58]. TAP [40–42] and SSITKA experiments [43] have indicated the Eley-Rideal character of this activation step. Methane activation is accounted for in the catalytic reaction mechanism through reaction (41) which produces the methyl radicals that can couple in the gas phase (reaction (9) in Table 2).

Reactions (42) and (43) are the hydrogen abstraction of ethane and ethylene, i.e., undesired consecutive reactions. Hydrogen abstraction of ethane on OCM catalyst has been observed by electron paramagnetic resonance (EPR) [53]. Although the C–H bonds in ethylene are a little stronger than in methane (Table 5), it is still likely that the hydrogen abstraction of ethylene also occurs on the catalyst surface. Hydrogen abstraction from ethylene leads to a vinyl radical, which is the main secondary source of carbon monoxide in the gas-phase reactions. The secondary reactions of ethylene on the catalyst surface also contribute to deep oxidation [11,59]. Through isotope labeling experiments, it has been determined that the rate constant for ethylene oxidation is three to eight times larger than that for methane direct oxidation [54,60,61].

Regeneration of active sites was assumed to occur through the formation and desorption of water, reactions (44) and (45), which is in line with the mechanism proposed by Lunsford and co-workers [6]. This description has also been used in several other microkinetic models [15,56,57]. The adsorption of hydroxyl radical on the same active site as the one for methane activation has been indicated by experiments [62] and observed by EPR [53]. TAP experiments [41] showed that the catalyst contains a pool of hydrogen atoms probably in the form of hydroxyl groups.

OCM catalysts cannot only be an activator leading to radical species, but also a scavenger of radicals [59]. In the homogeneous reactions of methane oxidative coupling, hydroperoxy radicals have been identified as a major carrier in the deep oxidation pathways of gas phase [39,63,64] and, hence, play a crucial role in the interplay between the catalytic reactions and the gas-phase reactions. Hydroperoxy radicals are highly susceptible to scavenging by the catalyst surface [65] and the reactor walls [66]. However, the exact elementary steps of the quenching effect have not been clearly revealed. Hence one irreversible step of quenching of hydroperoxy species [21], reaction (53), was adopted in the model to describe the quenching effect.

It has been well established that the heterogeneous deep oxidation acts as a major source for CO_2 formation. Several potential reaction pathways and corresponding elementary steps for direct CO_x formation on the catalyst surface have been proposed [11,59]. One is through the oxidation of methoxy surface species formed by methyl adsorption. Tong and Lunsford [67] showed that methyl radicals can be oxidized on the catalyst surface by feeding methyl radicals to a bed with a Li/MgO catalyst. The formation of methoxy over an Sm_2O_3 catalyst was also observed by infrared spectroscopy (IR) [68]. During an in situ IR study of OCM over lanthana catalysts, the existence of methoxy surface species has also been identified [50]. In previous microkinetic analyses [56,57], it was hypothesized that, once adsorbed, the methoxy species lead to carbon dioxide through a series of steps which are potentially infinitely fast. Furthermore, SSITKA experiments over Sn/Li/MgO [43] revealed that a surface species with a C-to-O ratio of 1 must be involved in the catalytic formation of carbon dioxide. Other possible routes of the catalytic oxidation of methyl radical include the formation of carboxyl surface species (COOH*) and formate (HCOO**) followed by the decomposition steps of these ones leading to CO_2 [36]. These routes prefer low temperature (<673 K) instead of high temperature (>1073 K) [36], which is necessary for OCM catalysts to achieve high activity. Furthermore, the C-to-O ratio of 1 cannot be met if these reaction routes were included in the catalytic reaction network. Thus, it is proposed that methoxy species degrade on the catalyst surface in the following sequence of reactions: $CH_3O^* \rightarrow H_2CO^* \rightarrow HCO^* \rightarrow CO^* \rightarrow CO_2^*$. This sequence corresponds to reactions (47)–(50), which describe the deep oxidation pathways of surface methoxy species in terms of elementary steps.

Carbon dioxide, as an undesired product, has a strong interaction with the catalysts by adsorbing on the catalyst surface. This interaction has been investigated through SSITKA experiments using carbon labeled carbon dioxide on different OCM catalysts [9,10,43]. The adsorption of CO_2 leads to the formation of carbonates on the catalyst surface, which have been identified by Fourier Transform IR and TPR experiments [12,69]. This adsorption occurs on the same active sites for OCM reactions [11] and, hence, decreases the conversion of methane. Therefore, the inhibition effect of CO_2 is included in the reaction network by reaction (52).

The catalytic oxidation of CO to CO_2 on OCM catalysts has been confirmed by comparing experiments in the absence and in the presence of a catalyst and by CO-oxidation experiments [70] and other studies [9]. CO can adsorb on the OCM catalyst to form CO* by reaction (51) [10], which is also the species involved in the oxidation sequence of methoxy.

4. Model parameter definition

4.1. Identification and implementation of catalyst descriptors

Special attention has been devoted to the incorporation of catalyst descriptors into the microkinetic model for methane oxidative coupling. This is expected to accelerate catalyst development by reducing the experimentation required in the assessment of new catalyst generations. The main advantage of a microkinetic model including catalyst descriptors is that it can quantify trends between reaction activity and selectivity on the one hand and catalyst properties on the other hand. As a result, such a model allows addressing which property of catalyst is the most relevant for the improvement of catalytic performance.

By extracting chemical information at the molecular level, it is possible to identify the key properties of different catalysts that strongly influence activity and selectivity of a reaction and, hence, provide a molecular-level basis for comparison between catalysts and further optimisation. This type of properties can be coined as

catalyst descriptors, which correspond to a measured or calculated physical or chemical property of the catalyst in interaction with the reacting species. The catalyst descriptor can affect the reaction parameter values, such as the activation energy and the reaction enthalpy. For instance, the descriptor can be an initial sticking probability, a bond energy of species or the density of active sites of a catalyst, etc. Incorporating one or several catalyst descriptors in a kinetic model enables the evaluation of the catalytic behaviour of a set of catalysts. It also results in the ability to relate the catalyst performance with the intrinsic catalyst properties via the reaction kinetics. The latter ability has long been desired by catalyst researchers as a guiding tool for new catalyst development. In a microkinetic analysis of the water-gas shift reaction, the adsorption enthalpies of carbon monoxide and oxygen that can describe the trend of reactivity of different catalysts have been extracted from the relative chemisorption energies [71].

The identification of catalyst descriptors for methane oxidative coupling starts from the microkinetic analysis of the reaction mechanism, which is based on the catalytic cycle concept and the thermodynamic consistency within such a cycle. Although the exact mechanism of the surface reactions on catalysts for methane oxidative coupling is still a matter of debate, several parallel reaction cycles have been identified on the catalyst surface: hydrogen abstraction of C_1 and C_2 species to produce radicals, deep oxidation of methyl radicals and of carbon monoxide. Within such a catalytic cycle, the reaction enthalpies of all elementary steps but one are calculated from literature data or taken as catalyst descriptor. The last reaction enthalpy is then obtained from thermodynamic consistency. In general, gas-phase reaction enthalpies are calculated from literature data, while chemisorption enthalpies are taken as catalyst descriptors. The surface reaction enthalpy is then the parameter that is obtained from the others through thermodynamic consistency. In what follows two examples are worked out, i.e., one for the hydrogen abstraction from methane and another for the deep oxidation of the methyl radical.

4.1.1. Hydrogen abstraction from methane, ethane and ethylene

In the hydrogen abstraction from methane, vide Fig. 2, there are three surface species: O*, OH* and H_2O*. From the energetic point of view, the standard enthalpy of formation of a surface species determines the reaction thermodynamics of the forward and backward elementary steps in which this species is involved. The standard enthalpy of formation of a surface species is calculated from the standard enthalpy of formation of a gas species and the corresponding chemisorption enthalpy of the gas species adsorbed on the catalyst surface. Consequently, the chemisorption enthalpies of oxygen and water are identified as the catalyst descriptors, D_2 and D_7, respectively. For instance, the standard formation enthalpy of H_2O surface species is derived from the following equation:

$$\Delta H^{\circ}_{fH_2O*} = D_7 - \Delta H^{\circ}_{fH_2O} \tag{7}$$

where $\Delta H^{\circ}_{fH_2O*}$ is the standard formation enthalpy of H_2O surface species, H_2O*, $\Delta H^{\circ}_{fH_2O}$ is the standard formation enthalpy of H_2O in gas phase; The standard formation enthalpies of gas-phase species are calculated from Chemkin [47]. The standard enthalpy of formation of OH* is calculated from the method developed by Su et al. [20]. Because methane is activated on the catalyst surface through an Eley-Rideal mechanism [40–42], the reaction enthalpy of this reaction is also used as a catalyst descriptor, D_1.

With catalyst descriptor D_1, D_2 and D_7, the reaction enthalpy of the combination of hydroxyl surface species (reaction (44)) can be calculated from the thermodynamic information of gas-phase reactions that are the reaction of methane and oxygen to produce methyl radicals and water:

$$\begin{aligned} &2CH_4 + 0.5O_2 \rightleftharpoons CH_3^{\bullet} + H_2O, \quad \Delta H_{overall} \\ &\Delta H^{\circ}_{44} = \Delta H^{\circ}_{overall} - 2D_1 - 0.5D_2 - D_7 \end{aligned} \tag{8}$$

where $\Delta H^{\circ}_{overall}$ is calculated from the standard formation enthalpies of gas-phase species.

4.1.2. Deep oxidation reactions

Catalyst descriptors D_3, D_4 and D_5 are identified in the cycle of the deep oxidation of the methyl radicals and used to calculate the reaction enthalpy of the catalytic steps in the cycle. The calculation of the reaction enthalpy of elementary steps on surface starts from thermodynamic data of the corresponding gas components. Reaction (47), the oxidation of methoxy surface species, vide Fig. 3, is used as an example. The reaction enthalpy of reaction (47) is calculated from the standard formation enthalpies of surface species as Eq. (9).

$$\Delta H^{\circ}_{47} = \Delta H^{\circ}_{fOH*} + \Delta H^{\circ}_{fCH_2O*} - \Delta H^{\circ}_{fCH_3O*} - \Delta H^{\circ}_{fO*} \tag{9}$$

ΔH°_{fO*}, ΔH°_{fOH*}, $\Delta H^{\circ}_{CH_2O*}$ and $\Delta H^{\circ}_{fCH_3O*}$ are the standard formation enthalpies of O*, OH*, CH_2O* and CH_3O*, respectively. A catalyst descriptor is defined in the calculation of the standard formation enthalpy of CH_2O*, $\Delta H^{\circ}_{fCH_2E*}$, according to D_4, the chemisorption enthalpy of CH_2O, while the chemisorption enthalpies of CH_3O* and OH*, $\Delta H^{\circ}_{fCH_3O*}$ and ΔH°_{fOH*}, are calculated by the method introduced by Su et al. [20].

4.1.3. Adsorption and desorption steps, active site density

Apart from reaction enthalpies as catalyst descriptors, also pre-exponential factor related parameters have been identified as catalyst descriptors. For the adsorption of gas species in OCM initial sticking probabilities have been selected for the methyl radicals, oxygen, carbon monoxide, carbon dioxide, and water. In particular for the methyl radical, a strong catalyst effect on the non-selective

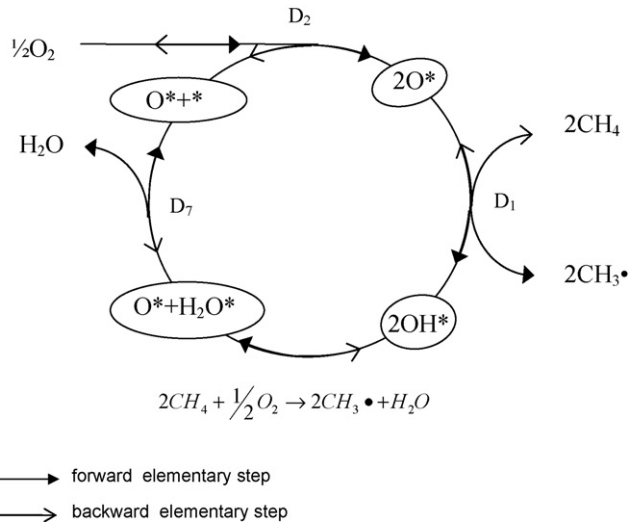

Fig. 2. A four step catalytic cycle for methyl radical production on an OCM catalyst.

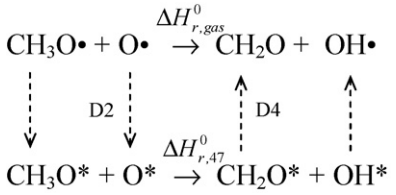

Fig. 3. A catalytic surface step of the oxidation of methoxy radical on an OCM catalyst.

oxidation leading to CO_2 has been reported [67]. In addition to these initial sticking probabilities, also the active site density is taken as a catalyst descriptor.

4.1.4. Summary of catalyst descriptors of OCM

In summary of the above sections, the set of catalyst descriptors in the microkinetic model for methane oxidative coupling can be classified as follows:

(a) Reaction enthalpy of hydrogen abstraction of CH_4 (D_1);
(b) Chemisorption enthalpies of O_2, CH_2O, HCO, CO, CO_2, H_2O (D_2–D_7);
(c) Initial sticking probabilities of O_2, $CH_3^{\bullet}$, CO, CO_2, H_2O (D_8–D_{12});
(d) Density of active sites (D_{13}).

As the reaction mechanism proposed for the microkinetic model has been defined at a molecular-level, it reflects the fundamental knowledge from experimental information and can be applied to different catalysts of methane oxidative coupling. The relevance of each of the descriptors in describing the catalyst effects on conversions and selectivities in OCM is discussed in Section 5.

4.2. Implementation of Polanyi relationships

The calculation of activation energies starting from the catalyst descriptors identified in Section 4.1 makes use of the Polanyi relationship, which relates the activation energy with the reaction enthalpy, the latter being obtained from the catalyst descriptors of OCM through thermodynamic consistency. A Polanyi relationship is used within a reaction family. The elementary reactions of methane oxidative coupling can be divided into four reaction families, each having a specific set of Polanyi parameters as shown in Table 4. With regard to the types of reactions, the similarity between the transition state and the products or reactants of each reaction family determines the value of the transfer coefficient α in the Polanyi relationship. CO catalytic oxidation to CO_2 (reaction (50)) and association of hydroxyl surface species to H_2O surface species (reaction (44)) cannot be classified into one of the two reaction families related to hydrogen abstraction as the structure variation of the two reactions are different. For the sake of generality, Polanyi relationships are also used for these two steps.

A kinetic analysis by Aparicio et al. [56] has shown that the activation energy of hydrogen abstraction of methane, ethane and ethylene is related with C–H bond energy as shown in Table 5. As the difference among the reaction enthalpies of reaction family 1 is determined by the difference in the C–H bond strengths (Q_{H-CH_3}, $Q_{H-C_2H_5}$ and $Q_{H-C_2H_5}$), the reaction enthalpies of hydrogen abstraction of ethane and ethylene, ΔH°_{42} and ΔH°_{43} are calculated with the catalyst descriptor D_1 by the following equations:

$$\Delta H^{\circ}_{42} = \Delta H^{\circ}_{41} + (Q_{H-C_2H_3} - Q_{H-CH_3}) = D_1 + 26.4 \quad (10)$$

$$\Delta H^{\circ}_{43} = \Delta H^{\circ}_{41} + (Q_{H-C_2H_5} - Q_{H-CH_3}) = D_1 - 15.9 \quad (11)$$

Table 4
Reactions families and corresponding parameter values for the Polanyi relationships used in the kinetic modeling of methane oxidative coupling

	Reaction family	α	E_0 (kJ mol^{-1})
1	Hydrogen abstraction by Eley-Rideal reaction (reactions (41)–(43))	0.75 [76]	144.2 ± 1.4
2	Hydrogen abstraction by surface reaction (reactions (47)–(49))	0.5 [32]	101.5 ± 1.2
3	Reaction (44)	0.65 [71]	73.9 ± 1.8
4	Reaction (50)	0.26 [35]	67.6 ± 3.3

E_0 was estimated from experimental data with 95% confidence interval.

Table 5
C–H bond energy [72] and activation energies of methane, ethane and ethylene

Component	C–H bond energy (kJ mol^{-1})	Activation energy of forward step of reaction family 1 (kJ mol^{-1})
Methane	438.9	145.2 (Reaction (41))
Ethane	423.0	133.3 (Reaction (42))
Ethylene	465.3	165.1 (Reaction (43))

where Q_{H-CH_3}, $Q_{H-C_2H_5}$ and $Q_{H-C_2H_3}$ are C–H bond energies of methane, ethane and ethylene, respectively [72].

Then the activation energies of the forward step of reaction family 1 are calculated as

$$E^{f}_{a,i} = E_{0,1} + \alpha_1 \Delta H^{\circ}_i \qquad (i = 41, 42, 43) \quad (12)$$

where α_1 is the Polanyi parameter of reaction family 1; $E^{f}_{a,i}$ is the activation energy of the forward step i in the reaction family 1; ΔH°_i is the reaction enthalpy of reaction i; $E_{0,1}$ is the intrinsic activation barrier of the Polanyi relationship for reaction family 1. The intrinsic activation barriers, E_0, of the reaction families were set as parameters that were estimated from the experimental data. For the corresponding backward elementary steps of reaction family 1, the activation energy is determined from the reaction enthalpy as

$$E^{b}_{a,i} = E^{f}_{a,i} - \Delta H^{\circ}_i \quad (13)$$

In catalytic reaction network of OCM (Table 3), the adsorption steps of gas species O_2, $CH_3^{\bullet}$, CO, CO_2, H_2O are assumed to be non-activated ones. Therefore, the activation energies of the adsorption steps are equal to zero and the rates are determined by the corresponding catalyst descriptors, i.e., the initial sticking probabilities of the gas-phase species. The activation energies of the desorption steps equal to the corresponding catalyst descriptors, i.e., chemisorption enthalpies of these surface species.

5. Parameter determination and discussion

Initial guesses for the catalyst descriptors were chosen within the range of physically reasonable values. As the catalyst descriptors of OCM have a corresponding physical or chemical meaning, the initial guesses and the final estimates must be within certain physical constraints. Otherwise, the microkinetic model fails to capture the essential surface chemistry [32]. For instance, the adsorption enthalpy of CO measured on MgO is 60–100 kJ mol^{-1} [73]. The adsorption enthalpy of O_2 on metal oxide is lower than 300 kJ mol^{-1} [74]. As OCM catalysts are basic, it is well known that CO_2 can adsorb on the catalyst surface and form strong bonds. The adsorption enthalpy of CO_2 measured on different metal oxides varies from 60 to 180 kJ mol^{-1} [75]. These values are used as constraints for the catalyst descriptors. During the calculation, the upper and lower bound of activation energy of catalytic reactions are set as 300 and 20 kJ mol^{-1}, respectively.

For reactions involving gas-phase molecules colliding with the surface, the maximum value of pre-exponential factors can be calculated from collision theory. The ultimate values for the pre-exponential factors equal this maximum value corrected by an initial sticking probability of gas molecules, which is generally experimentally measured. In this case, as there are no experimental data measured on the Sn/Li/MgO catalyst for O_2, CH_4, CO, CO_2 and H_2O, the initial sticking probabilities of these gas species are assumed to be 0.1 as first approximation. Based on experimental observations, the initial sticking probability for methyl radicals on different OCM catalysts varies in several magnitudes, from 10^{-4} to 10^{-7} [67]. The rate coefficient of the quenching reaction (53), adopted from Couwenberg's kinetic model [21], is fixed in the parameter estimation. For reactions involving only

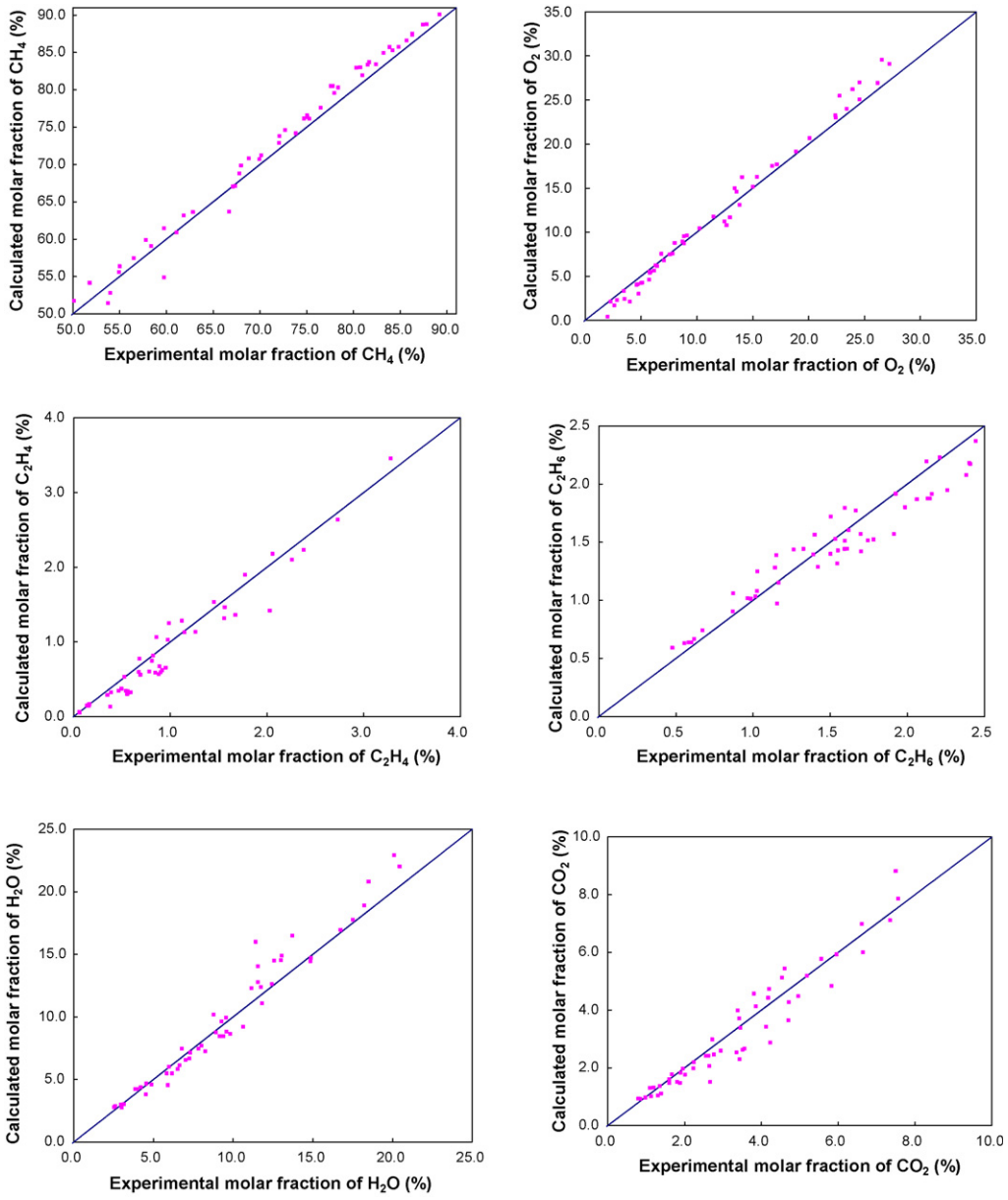

Fig. 4. Parity diagrams for CH_4, O_2, C_2H_4, C_2H_6, H_2O, CO_2. The experimental conditions are reported in Table 1. X_{CH_4}: 0.07–0.26; X_{O_2}: 0.20–0.98. Calculated molar fractions (●) are, calculated by the microkinetic model shown in Tables 2 and 3 with the corresponding Eqs. (4)–(6) and the reactor model introduced in Section 2.2. Parameters in Table 3 are calculated from Eqs. (7) to (13) and the values of catalyst descriptors of Sn/Li/MgO listed in Table 6.

surface species, pre-exponential factors were determined by comparing the reactant's mobility with that of the transition state. For instance, for the association step of O* to O_2 in reaction (40), $O^* + O^* \rightarrow O_2 + 2^*$, it was assumed that atomic oxygen is immobile on the catalyst surface. Therefore, the pre-exponential factor A in Eq. (4) can be calculated as follows [32]:

$$A_b^{40} = \frac{k_b T}{h}\frac{1}{\sigma} = 2.39 \times 10^{15}\ \mathrm{m^2\ mol\ s^{-1}} \quad (14)$$

where A_b^{40} is the pre-exponential factor of the reverse step of reaction (40); k_b is Boltzmann constant, J K^{-1}; h is Plank constant, J s^{-1}.

It has been known that the conversion and selectivity of OCM varies with the density of active sites of OCM catalyst [57]. The density of active sites of OCM catalysts can be evaluated from the transient kinetics or particle modeling [50]. The maximum value, 1.14×10^{-5} mol m^{-2}, is assumed for the density of active sites on the catalyst surface and fixed during the parameter estimation using the data obtained on the Sn promoted LiMgO [20]. For the non-promoted Li/MgO the active site density, D_{13}, was estimated by regression.

Krylov [76] has found a transfer coefficient value of $\alpha = 0.75$ for hydrogen-abstraction reactions, i.e. reaction family 1, on several OCM catalysts. In the simulation of the catalytic partial oxidation of methane, Dumesic et al. [32] used $\alpha = 0.5$ for the elementary steps similar to the reactions in the reaction family 2. The other α-coefficients are also determined from the literature. As an exothermic reaction, the association of CO* and O* to CO_2* was assumed to having an early transition state, which is reflected in the α-value of 0.26 as found by theoretical calculations [35]. The value $\alpha = 0.65$ is used for the association of hydroxyl surface species, reactions (44) [71].

Simulation of experiments was performed using the above kinetic model and the estimated catalyst descriptors, combined with the gas-phase model and the reactor model described in

Table 6
Estimates for the catalyst descriptors of Li/MgO and Sn/Li/MgO catalysts for OCM

	Catalyst descriptor	Value
D_1	Reaction enthalpy of hydrogen abstraction of CH_4 (kJ mol^{-1})	61.4 ± 0.8
D_2	Chemisorption enthalpy of O_2 (kJ mol^{-1})	110.7 ± 3.0
D_3	Chemisorption enthalpy of CH_2O (kJ mol^{-1})	91.7 ± 4.2
D_4	Chemisorption enthalpy of HCO (kJ mol^{-1})	233.6 ± 15.6
D_5	Chemisorption enthalpy of CO (kJ mol^{-1})	101.4 ± 2.0
D_6	Chemisorption enthalpy of CO_2 (kJ mol^{-1})	160.9 ± 3.4
D_7	Chemisorption enthalpy of H_2O (kJ mol^{-1})	54.2 ± 2.0
D_8	Initial sticking probability of O_2	0.4 ± 0.01
D_9	Initial sticking probability of $CH_3^{\bullet}$	$3.3 \pm 0.2 \times 10^{-5}$, $1.21 \pm 0.1 \times 10^{-3}$
D_{10}	Initial sticking probability of CO	$2.7 \pm 0.3\ 10^{-4}$
D_{11}	Initial sticking probability of CO_2	0.013 ± 0.002
D_{12}	Initial sticking probability of H_2O	0.52 ± 0.03
D_{13}	Density of active sites (mol m^{-2})	$2.45 \pm 0.2 \times 10^{-6}$, 1.14×10^{-5}

Value ± 95% confidence interval. Final weighted sums of squares = 9.65; *F*-value for significance of the regression = 618.3; *F* tabulated value = 2.79.

Section 2. The experimental data were obtained from literature [46] and the optimisation tools have been described in Section 2. The catalyst descriptor values for Sn/Li/MgO as well as the corresponding statistics are shown in Table 6. The maximum absolute value in the correlation coefficient matrix amounts to 0.75 and occurs between D_7 and D_9, which allows concluding that no significant correlation between the adjustable parameters occurs. With a value of 618.3 for the global significance of the regression, the model's adequacy is illustrated.

The microkinetic model including the set of catalyst descriptors given in Table 6 yielded an excellent agreement with the experimental data on the Sn promoted Li/MgO catalyst, as shown in the parity plots (Fig. 4) of the various OCM products for the complete range of experimental conditions used for the parameter estimation, vide Fig. 5. Fig. 6 shows the conversions of methane and oxygen and the selectivities towards C_2 and CO_x versus the inlet methane-to-oxygen molar ratio, which illustrates that a one-step

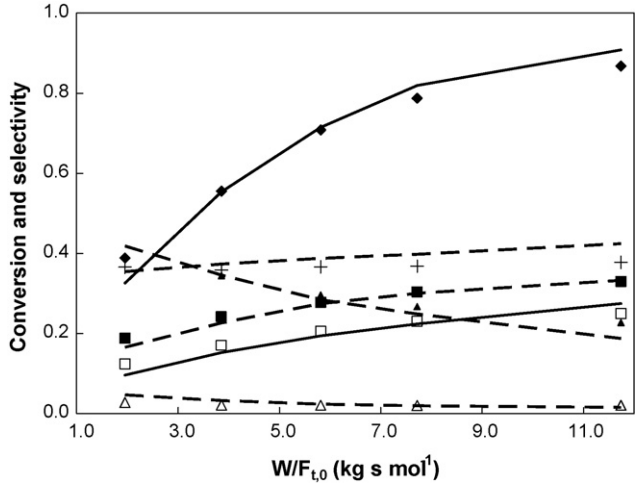

Fig. 5. Methane and oxygen conversions and product selectivities vs. space time. Lines: calculated conversions (–) and selectivities (- -), calculated by the microkinetic model shown in Tables 2 and 3 with the corresponding Eqs. (4)–(6) and the reactor model introduced in Section 2.2. Parameters in Table 3 are calculated from Eqs. (7) to (13) and the values of catalyst descriptors of Sn/Li/MgO listed in Table 5. Points—experiments: (◆) O_2; (+) CO_2; (▲) C_2H_6; (■) C_2H_4; (□) CH_4; (△) CO. Experimental conditions: T = 973 K, P = 110 kPa, and CH_4/O_2 = 3.0.

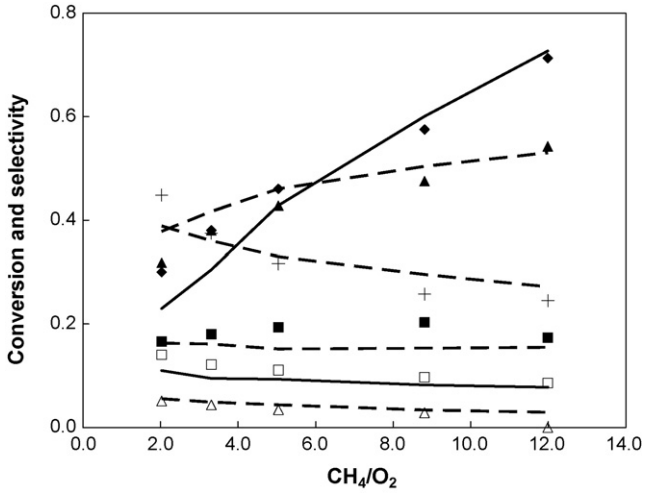

Fig. 6. Methane and oxygen conversions and product selectivities vs. CH_4/O_2. Lines: calculated conversions (–) and selectivities (- -), calculated by the microkinetic model shown in Tables 2 and 3 with the corresponding Eqs. (4)–(6) and the reactor model introduced in Section 2.2. Parameters in Table 3 are calculated from Eqs. (7) to (13) and the values of catalyst descriptors of Sn/Li/MgO listed in Table 5. Points—experiments: (◆) O_2; (+) CO_2; (▲) C_2H_6; (■) C_2H_4; (□) CH_4; (△) CO. Experimental conditions: T = 1013 K, P = 130 kPa, and $W/F_{t,0}$ = 2.0.

oxygen adsorption is sufficient to adequately simulate the experimental data. The accurate simulation of the selectivities towards carbon dioxide shows that reactions (45)–(49) capture the trend of the primary carbon dioxide production. A slight under-prediction of the conversion at lower CH_4/O_2 ratios may indicate that the model calculated rates for methane activation by oxygen are on the low side. That the model also adequately describes experiments at 948, 973, and 1013 K, can be seen in Fig. 7, where the conversions of methane and oxygen are plotted versus the inlet methane-to-oxygen ratio. This gives confidence in the constructed reaction mechanism and the corresponding activation energies.

As the simulations calculated by the microkinetic model with the catalyst descriptors show a good agreement with the experimental data of Sn/Li/MgO, it proves that the reaction

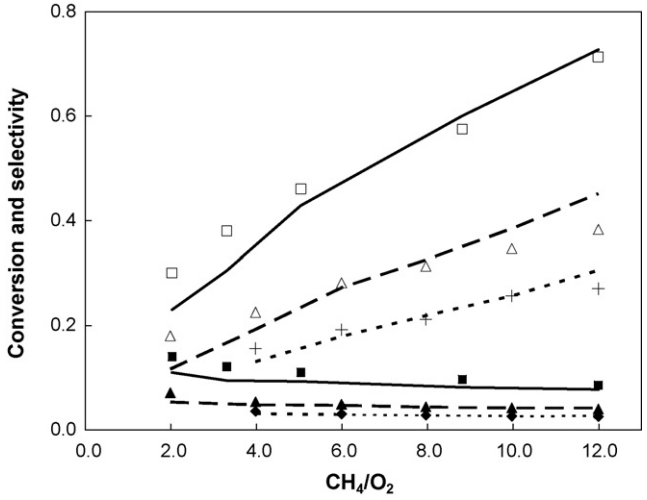

Fig. 7. Methane and oxygen conversions and product selectivities vs. CH_4/O_2. Lines: calculated conversions and selectivities at different temperatures: (—) 1013 K; (– –) 973 K; (- - -) 944 K, calculated by the microkinetic model shown in Tables 2 and 3 with the corresponding Eqs. (4)–(6) and the reactor model introduced in Section 2.2. Parameters in Table 3 are calculated from Eqs. (7) to (13) and the values of catalyst descriptors of Sn/Li/MgO listed in Table 5. Points—experiments: Conversion of O_2 (□) 1013 K; (△) 973 K; (+) 944 K. Conversion of CH_4 (◆) 944 K; (▲) 973 K; (■) 1013 K. Experimental conditions: P = 130 kPa, and $W/F_{t,0}$ = 2.0.

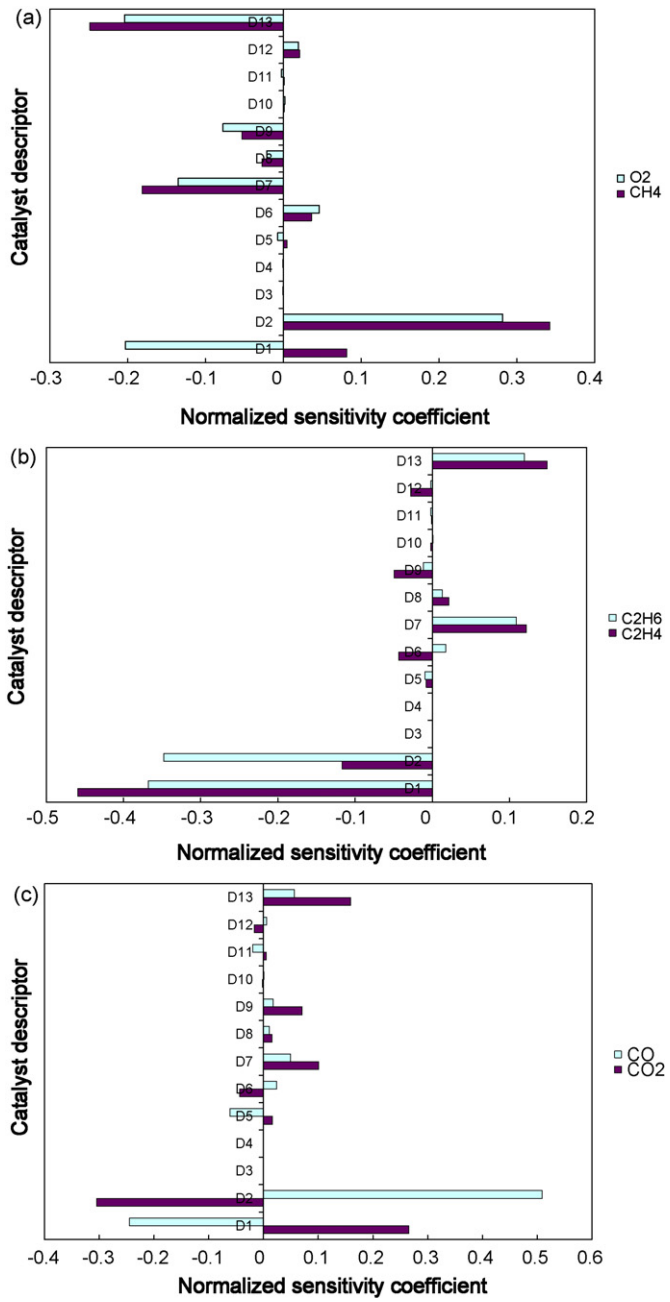

Fig. 8. Sensitivity analysis of catalyst descriptors with the microkinetic model of OCM, (a) for CH_4 and O_2; (b) for C_2H_4 and C_2H_6; and (c) for CO and CO_2. D_1, reaction enthalpy of CH_4 hydrogen abstraction; D_2, chemisorption enthalpy of oxygen; D_3, chemisorption enthalpy of CH_2O; D_4, chemisorption enthalpy of HCO; D_5, chemisorption enthalpy of CO; D_6, chemisorption enthalpy of CO_2; D_7, chemisorption enthalpy of H_2O; D_8, initial sticking probability of O_2; D_9, initial sticking probability of $CH_3^{\bullet}$; D_{10}, initial sticking probability of CO; D_{11}, initial sticking probability of CO_2, D_{12}, initial sticking probability of CO_2, D_{13}, density of active sites. Operating conditions: T, 973 K; P, 110 kPa; $W/F_{t,0}$, 3.1 kg s mol^{-1}; CH_4/O_2, 3.0; catalyst, Sn/Li/MgO. Sensitivity coefficients are calculated from Eq. (3) with the value of catalyst descriptors in Table 6 and the microkinetic model shown in Tables 2 and 3.

mechanism proposed can accurately describe the initiation of methyl radical and the later deep oxidation steps. It also considers the catalytic hydrogen abstraction of C_2H_4 by reaction (42). When the conversion of CH_4 is high, C_2H_4 decomposes into radicals and the C_2 selectivity decreases. The values of catalyst descriptors are also located within the range of literature data, for instance, the reaction enthalpy of hydrogen abstraction of methane for Sn/Li/MgO, 61.4 kJ mol^{-1}, is within the range from 58.0 [77] to 74.0 kJ mol^{-1} [78].

The simulations performed with the microkinetic model indicate that these catalyst descriptors can capture the fundamental chemistry of catalyst. For future catalyst development, it would be convenient to know which catalyst descriptors are the most important and how they affect the reactions. The information obtained can be used as a guideline to direct the development of OCM catalyst. Fig. 8 shows the sensitivity analysis of catalyst descriptors for CH_4, O_2, C_2H_4, C_2H_6, CO and CO_2, performed at the temperature of 973 K and the methane/oxygen ratio of 2.0. The results reveal that the conversion of CH_4 and O_2 and the selectivities towards C_2H_4, C_2H_6, CO and CO_2 are strongly affected by the reaction enthalpy of methane hydrogen abstraction (D_1) and the chemisorption enthalpy of oxygen (D_2). This indicates they roles in the reaction mechanism of the oxygen surface species (reaction (40)) and the methyl radicals (reaction (41)), which is consistent with the many experiments reported in the literature [20,54,58]. The density of active sites (D_{13}) is an important property of OCM catalysts as it affects all catalytic steps of OCM. The effects of the chemisorption enthalpy of CO_2 (D_6), chemisorption enthalpy of H_2O (D_7) and initial sticking probability of $CH_3^{\bullet}$ (D_9) are less pronounced. D_6 represents the inhibition effect of CO_2 by the adsorption of CO_2 on active sites. D_7 relates with the adsorption of H_2O, which also affects the concentration of oxygen surface species. D_9 affects the consumption rate of $CH_3^{\bullet}$ by reaction (46).

The data obtained on the non-promoted Li/MgO catalyst have been assessed through the same kinetic model in which, starting from the values obtained on the promoted catalyst, only two catalyst descriptors were adjusted by regression. These two catalyst descriptors were the initial sticking probability of $CH_3^{\bullet}$ (D_9) and the density of active sites (D_{13}). According to the study of Li/MgO and Sn/Li/MgO [21,41], the assumption was made that the same reaction mechanism can be applied to these two catalysts and the main difference between them is situated in the density of active sites, D_{13}. The sensitivity analysis of conversion and selectivities on the catalyst descriptors identified, D_{13} as an effective catalyst descriptor determining mainly the conversions. The initial sticking probability of the methyl radical, D_9, may vary significantly with the composition of catalyst [58]. Hence, despite its mild effect observed in the sensitivity analysis, this descriptor is also selected for adjustment to the data on the non-promoted catalyst. Other catalyst descriptors are fixed at the values of Sn/Li/MgO. In Fig. 9, the simulations of Li/MgO are in a good agreement

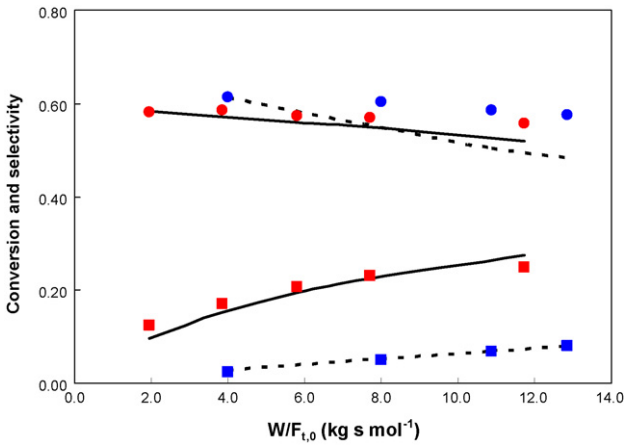

Fig. 9. Conversion and selectivity vs. space time. Lines: calculated conversions and selectivities (- -) Li/MgO; (–) Sn/LiMgO. Points—experiments: (■) CH_4, and (●) C_2. Experimental conditions: LiMgO, T = 1073 K, P = 112 kPa, CH_4/O_2 = 4.0; Sn/LiMgO, T = 1012 K, P = 110 kPa, and CH_4/O_2 = 2.0.

with the experiments. The maximum conversion of methane with Sn/Li/MgO is 0.24 at 1012 K, while with Li/MgO the maximum conversion is limited to 0.1 even at a higher temperature, 1073 K. At the maximum conversion of methane, the C_2 selectivity of both catalysts is close to 0.6. It is observed that Sn/Li/MgO is more effective than Li/MgO. From Li/MgO to Sn/Li/MgO, the increase of D_{13} and the decrease of D_9 may represent the promoting effect of Sn, which increases the density of active sites [41,43] and decreases the oxidation rate of methyl radicals.

The results indicate that the reaction enthalpy of methane hydrogen abstraction (D_1) and the chemisorption enthalpy of oxygen (D_2) are the key catalyst descriptors for describing the OCM behaviour on wider range of catalysts. This is in agreement with the conclusion derived from an analysis of surface energetics of OCM catalysts [20]. The effects of these two catalyst descriptors on OCM reactions and the optimisation of OCM catalysts will be the target of the future work.

6. Conclusions

The adequate description of the complex chemistry involved in oxidative coupling of methane requires a heterogeneous reactor model explicitly accounting for the interactions between gas phase and catalytic reactions. A kinetic model accounting for all reactions in terms of elementary steps provides several advantages, the most important one being the ability to link reaction parameter values such as the activation energy or the elementary reaction enthalpy with so-called catalyst descriptors. The use of catalyst descriptors in combination with semi-empirical expressions such as the Polanyi relationship allows reducing the number of adjustable kinetic parameters in the model. Typical catalyst descriptors are related to elementary steps accounting for interaction between gas-phase molecules and the catalytic surface. Hence, chemisorption enthalpies, initial sticking probabilities and Eley-Rideal reaction enthalpy are used as catalyst descriptors in addition to the active site density. The simulations of two catalysts of OCM indicate catalyst descriptor provide the capability to capture the chemical information from experiments of different catalysts. The sensitivity analysis reveals the important catalyst descriptors on OCM catalysts that are consistent with the previous reports. Hence, a microkinetic model including catalyst descriptors may provide guidelines for high-throughput catalyst development.

Acknowledgement

This work was supported by the European research project "TOPCOMBI" (contract NMP2-CT2005-515792).

References

[1] G.E. Keller, M.M. Bhasin, J. Catal. 73 (1982) 9.
[2] O.V. Krylov, Catal. Today 13 (1992) 481.
[3] K.D. Campbell, J.H. Lunsford, J. Phys. Chem. 92 (1988) 5792.
[4] K.D. Campbell, E. Morales, J.H. Lunsford, J. Am. Chem. Soc. 109 (1987) 7900.
[5] D.J. Driscoll, W. Martir, J.X. Wang, J.H. Lunsford, J. Am. Chem. Soc. 107 (1985) 58.
[6] T. Ito, J.X. Wang, C.H. Lin, J.H. Lunsford, J. Am. Chem. Soc. 107 (1985) 5062.
[7] P.F. Nelson, C.A. Lukey, N.W. Cant, J. Phys. Chem. 92 (1988) 6176.
[8] C.H. Lin, T. Ito, J.X. Wang, J.H. Lunsford, J. Am. Chem. Soc. 109 (1987) 4808.
[9] K.P. Peil, J.G. Goodwin, G. Marcelin, J. Phys. Chem. 93 (1989) 5977.
[10] K.P. Peil, J.G. Goodwin, G. Marcelin, J. Catal. 131 (1991) 143.
[11] G.A. Martin, C. Mirodatos, Fuel Process. Technol. 42 (1995) 179.
[12] J. Galuszka, Catal. Today 21 (1994) 321.
[13] M.T. Xu, T.H. Ballinger, J.H. Lunsford, J. Phys. Chem. 99 (1995) 14494.
[14] Y. Simon, R. Baronnet, G.M. Côme, P.M. Marquaire, Nat. Gas Convers. 147 (Vii) (2004) 571.
[15] Y. Simon, F. Baronnet, P.M. Marquaire, Ind. Eng. Chem. Res. 46 (2007) 1914.
[16] M.Y. Sinev, Catal. Today 13 (1992) 561.
[17] M.Y. Sinev, Catal. Today 24 (1995) 389.
[18] D. Wolf, M. Heber, W. Grunert, M. Muhler, J. Catal. 199 (2001) 92.
[19] D. Wolf, M. Slinko, E. Kurkina, M. Baerns, Appl. Catal. A: Gen. 166 (1998) 47.
[20] Y.S. Su, J.Y. Ying, W.H. Green, J. Catal. 218 (2003) 321.
[21] P.M. Couwenberg, Q. Chen, G.B. Marin, Ind. Eng. Chem. Res. 35 (1996) 3999.
[22] P.M. Couwenberg, Q. Chen, G.B. Marin, Ind. Eng. Chem. Res. 35 (1996) 415.
[23] S. Senkan, Angew. Chem. Int. Ed. 40 (2001) 312–329.
[24] R.J. Hendershot, C.M. Snively, J. Lauterbach, Chem. Eur. J. 11 (2005) 806–814.
[25] A. Corma, J.M. Serra, Catal. Today 107/108 (2005) 3.
[26] W.F. Maier, K. Stowe, S. Sieg, Angew. Chem. Int. Ed. 46 (2007) 6016–6067.
[27] A. Holzwarth, P. Denton, H. Zanthoff, C. Mirodatos, Catal. Today 67 (2001) 309–318.
[28] J.M. Caruthers, J.A. Lauterbach, K.T. Thomson, V. Venkatasubramanian, C.M. Snively, A. Bhan, S. Katare, G. Oskarsdottir, J. Catal. 216 (2003) 98.
[29] A. Corma, J.M. Serra, P. Serna, M. Moliner, J. Catal. 232 (2005) 335–341.
[30] A.C. van Veen, D. Farrusseng, M. Rebeilleau, T. Decamp, A. Holzwarth, Y. Schuurman, C. Mirodatos, J. Catal. 216 (2003) 135.
[31] M. Boudart, Catal. Lett. 65 (2000) 1.
[32] J.A. Dumesic, D.F. Rudd, L.M. Aparicio, J.E. Rekoske, The Microkinetics of Heterogeneous Catalysis, American Chemical Society, Washington, DC, 1993, 316.
[33] A.A. Gokhale, S. Kandoi, J.P. Greeley, M. Mavrikakis, J.A. Dumesic, Chem. Eng. Sci. 59 (2004) 4679.
[34] J.K. Norskov, T. Bligaard, A. Logadottir, S. Bahn, L.B. Hansen, M. Bollinger, H. Bengaard, B. Hammer, Z. Sljivancanin, M. Mavrikakis, Y. Xu, S. Dahl, C.J.H. Jacobsen, J. Catal. 209 (2002) 275.
[35] A. Michaelides, Z.P. Liu, C.J. Zhang, A. Alavi, D.A. King, P. Hu, J. Am. Chem. Soc. 125 (2003) 3704.
[36] A.B. Mhadeshwar, H. Wang, D.G. Vlachos, J. Phys. Chem. B 107 (2003) 12721.
[37] H.L. Zhang, J.J. Wu, S. Qin, C.W. Hu, Ind. Eng. Chem. Res. 45 (2006) 7090.
[38] Q. Chen, J.H.B.J. Hoebink, G.B. Marin, Ind. Eng. Chem. Res. 30 (1991) 2088.
[39] Q. Chen, P.M. Couwenberg, G.B. Marin, AICHE J. 40 (1994) 521.
[40] J.T. Gleaves, J.R. Ebner, T.C. Kuechler, Catal. Rev. Sci. Eng. 30 (1988) 49–116.
[41] E.P.J. Mallens, J.H.B.J. Hoebink, G.B. Marin, J. Catal. 160 (1996) 222.
[42] O.V. Buyevskaya, M. Rothaemel, H.W. Zanthoff, M. Baerns, J. Catal. 150 (1994) 71.
[43] R.H. Nibbelke, J. Scheerova, M.H.J.M. de Croon, G.B. Marin, J. Catal. 156 (1995) 106.
[44] H.H. Rosenbrock, Comput. J. 3 (1960) 175.
[45] Netlib, http://www.netlib.org.
[46] P.W. Cowenberg, Kinetic studies of methane oxidative coupling, PhD Dissertation, Einhoven University, Einhoven, 1995.
[47] R.J. Kee, F.M. Rupley, J.A. Miller, M.E. Coltrin, J.F. Grcar, E. Meeks, H.K. Moffat, A.E. Lutz, G. Dixon-Lewis, M.D. Smooke, J. Warnatz, G.H. Evans, R.S. Larson, R.E. Mitchell, L.R. Petzold, W.C. Reynolds, M. Caracotsios, W.E. Stewart, P. Glarborg, H. Wang, O. Adigun, W.G. Houf, C.P. Chou, S.F. Miller, P. Ho, D.J. Young, CHEMKIN Release 4. 0, Reaction Design, Inc., San Diego, CA, 2004.
[48] V.T. Amorebieta, A.J. Colussi, J. Phys. Chem. 92 (1988) 4576.
[49] P.J. Gellings, H.J.M. Bouwmeester, Catal. Today 58 (2000) 1.
[50] S. Lacombe, C. Geantet, C. Mirodatos, J. Catal. 151 (1995) 439.
[51] S. Lacombe, H. Zanthoff, C. Mirodatos, J. Catal. 155 (1995) 106.
[52] A.M. Maitra, Applied, Catal. A: Gen. 104 (1993) 11.
[53] M.C. Paganini, M. Chiesa, P. Martino, E. Giamello, E. Garrone, J. Phys. Chem. B 107 (2003) 2575.
[54] S. Pak, P. Qiu, J.H. Lunsford, J. Catal. 179 (1998) 222.
[55] Y.D. Tong, J.H. Lunsford, J. Chem. Soc. Chem. Commun. (1990) 792.
[56] L.M. Aparicio, S.A. Rossini, D.G. Sanfilippo, J.E. Rekoske, A.A. Trevino, J.A. Dumesic, Ind. Eng. Chem. Res. 30 (1991) 2114.
[57] J.G. McCarty, Mechanism of Cooxidative Methane Dimerization Catalysis: Kinetic and Thermodynamic Aspects, Van Nostrand Reinhold, New York, 1992, p. 320.
[58] J.H. Lunsford, Langmuir 5 (1989) 12.
[59] J.H. Lunsford, Formation and Reactions of Methyl Radicals over Metal Oxide Catalysts, Van Nostrand Reinhold, New York, 1992, p. 3.
[60] C.L. Shi, M.P. Rosynek, J.H. Lunsford, J. Phys. Chem. 98 (1994) 8371.
[61] W.Y. Tung, L.L. Lobban, Ind. Eng. Chem. Res. 31 (1992) 1621.
[62] K.B. Hewett, L.C. Anderson, M.P. Rosynek, J.H. Lunsford, J. Am. Chem. Soc. 118 (1996) 6992.
[63] C.A. Mims, R. Mauti, A.M. Dean, K.D. Rose, J. Phys. Chem. 98 (1994) 13357.
[64] M. Machli, C. Boudouris, S. Gaab, J. Find, A.A. Lemonidou, J.A. Lercher, Catal. Today 112 (2006) 53.
[65] J. Sanchezmarcano, C. Mirodatos, E.E. Wolf, G.A. Martin, Catal. Today 13 (1992) 227.
[66] R. Martin, M. Niclause, G. Scacchi, Industrial laboratory pyrolyses, in: L.F. Albright, B.L. Crynes (Eds.), Proceedings of the ACS Symposium Series, 1976, p. 37.
[67] Y.D. Tong, J.H. Lunsford, J. Am. Chem. Soc. 113 (1991) 4741.
[68] Y. Sakata, T. Arimoto, N. Miharu, H. Imamura, Chem. Commun. (2001) 1810.
[69] Y.D. Xu, L. Yu, X.X. Guo, Appl. Catal. A: Gen. 164 (1997) 47.
[70] K. van der Wiele, J.W.H.M. Geerts, J.M.N. van Kasteren, in: E.E. Wolf (Ed.), Methane Conversion by Oxidative Processes, Van Nostrand Reinhold, New York, 1992, p. 259.
[71] N. Schumacher, A. Boisen, S. Dahl, A.A. Gokhale, S. Kandoi, L.C. Grabow, J.A. Dumesic, M. Mavrikakis, I. Chorkendorff, J. Catal. 229 (2005) 265.
[72] D.R. Lide, CRC Handbook of Chemistry and Physics, CRC Press LLC, 2004.
[73] A. Zecchina, D. Scarano, S. Bordiga, G. Spoto, C. Lamberti, Adv. Catal. 46 (2002) 265.
[74] Y.P. Arnaud, Appl. Surf. Sci. 62 (1992) 37.
[75] A. Auroux, A. Gervasini, J. Phys. Chem. 94 (1990) 6371.
[76] O.V. Krylov, Catal. Today 18 (1993) 209.
[77] M.A. Johnson, E.V. Stefanovich, T.N. Truong, J. Phys. Chem. B 101 (1997) 3196–3201.
[78] C.R.A. Catlow, S.A. French, A.A. Sokol, J.M. Thomas, Philos. Trans. R. Soc. A: Math. Phys. Eng. Sci. 363 (2005) 913–936.